

**Quantum Chemistry**

# Quantum Nuclear Delocalization and its Rovibrational Fingerprints

*Irén Simkó, Christoph Schran, Fabien Briec, Csaba Fábri, Oskar Asvany, Stephan Schlemmer, Dominik Marx,\* and Attila G. Császár\**

**Abstract:** Quantum mechanics dictates that nuclei must undergo some delocalization. In this work, emergence of quantum nuclear delocalization and its rovibrational fingerprints are discussed for the case of the van der Waals complex  $\text{HHe}_3^+$ . The equilibrium structure of  $\text{HHe}_3^+$  is planar and T-shaped, one He atom solvating the quasi-linear  $\text{He}-\text{H}^+-\text{He}$  core. The dynamical structure of  $\text{HHe}_3^+$ , in all of its bound states, is fundamentally different. As revealed by spatial distribution functions and nuclear densities, during the vibrations of the molecule the solvating He is not restricted to be in the plane defined by the instantaneously bent  $\text{HHe}_2^+$  chromophore, but freely orbits the central proton, forming a three-dimensional torus around the  $\text{HHe}_2^+$  chromophore. This quantum delocalization is observed for all vibrational states, the type of vibrational excitation being reflected in the topology of the nodal surfaces in the nuclear densities, showing, for example, that intramolecular bending involves excitation along the circumference of the torus.

as proton<sup>[2-4]</sup> and heavy-atom<sup>[5,6]</sup> tunneling come to the fore. Such nuclear quantum effects (NQE)<sup>[7]</sup> in chemistry emerge as manifestations of the ‘wave-particle duality’ of nature. Yet, the underlying NQEs are mostly thought of and treated in terms of semi- and quasi-classical pictures, which all remain, as much as possible, close to the concept of classical motion of pointlike particles – the wavelike properties of nuclei being swept under the rug. Nevertheless, there are notable examples which defy, due to wavelike properties of the nuclei, the notion of a localized chemical structure: protonated acetylene,<sup>[8-10]</sup> protonated methane,<sup>[11-14]</sup> and the hydrated proton.<sup>[15]</sup> *Ab initio* path integral molecular dynamics (PIMD)<sup>[16,17]</sup> calculations provided insight into the dynamics of these systems, for example, by the analysis of nuclear spatial distribution functions (SDF). Still, nuclear delocalization that encompasses the entire molecular framework, akin to electron delocalization within molecules, as well as its impact on the rovibrational excitations remain largely *terra incognita* even today.

To present a case when one atom exhibits delocalization with respect to all the other atoms of the molecule, we carried out a structural, dynamical, and spectroscopic study of the van der Waals (vdW) complex  $\text{HHe}_3^+$ , a fascinating member of the ‘He-solvated proton’ ( $\text{HHe}_n^+$ ) family.<sup>[18-20]</sup>  $\text{HHe}_3^+$  has a single minimum on its Born–Oppenheimer potential energy surface (PES) (with three versions corresponding to the different permutations of the He atoms). The corresponding equilibrium structure is characterized by a quasi-linear triatomic core (also called ‘chromophore’),  $\text{He}-\text{H}^+-\text{He}$ , and a ‘solvating’ He atom, in a planar T-shaped arrangement (see the global minimum (GM) inset in Figure 1a). The solvating He atom is expected to execute large-amplitude motion due to the weakness of the vdW

## 1. Introduction

Delocalization of electrons within molecules, allowed by their ‘wavelike’ nature, is a concept widely utilized in chemistry. It suffices to refer to such chemical terms as ‘aromatic rings’, ‘resonance structures’, and ‘delocalization energies’, all covered in textbooks on organic chemistry.<sup>[1]</sup> When it comes to quantum delocalization of nuclei, in particular in the vibrational ground state, phenomena such

[\*] I. Simkó, A. G. Császár

Laboratory of Molecular Structure and Dynamics, Institute of Chemistry, ELTE Eötvös Loránd University, H-1117 Budapest, Pázmány Péter sétány 1/A, Hungary  
 E-mail: attila.csaszar@ttk.elte.hu

I. Simkó, C. Fábri, A. G. Császár  
 MTA-ELTE Complex Chemical Systems Research Group, H-1117 Budapest, Pázmány Péter sétány 1/A, Hungary

I. Simkó  
 Hevesy György PhD School of Chemistry, ELTE Eötvös Loránd University, H-1117 Budapest, Pázmány Péter sétány 1/A, Hungary

C. Schran, F. Briec, D. Marx  
 Lehrstuhl für Theoretische Chemie, Ruhr-Universität Bochum, 44780 Bochum, Germany  
 E-mail: dominik.marx@theochem.ruhr-uni-bochum.de

C. Schran

Present address: Yusuf Hamied Department of Chemistry, University of Cambridge, Lensfield Road, Cambridge, CB2 1EW, UK

F. Briec

Present address: Laboratoire Matière en Conditions Extrêmes, Université Paris-Saclay, CEA, DAM, DIF, 91297 Arpajon, France

O. Asvany, S. Schlemmer

I. Physikalisches Institut, Universität zu Köln, Zùlpicher Str. 77, 50937 Köln, Germany

© 2023 The Authors. Angewandte Chemie International Edition published by Wiley-VCH GmbH. This is an open access article under the terms of the Creative Commons Attribution License, which permits use, distribution and reproduction in any medium, provided the original work is properly cited.

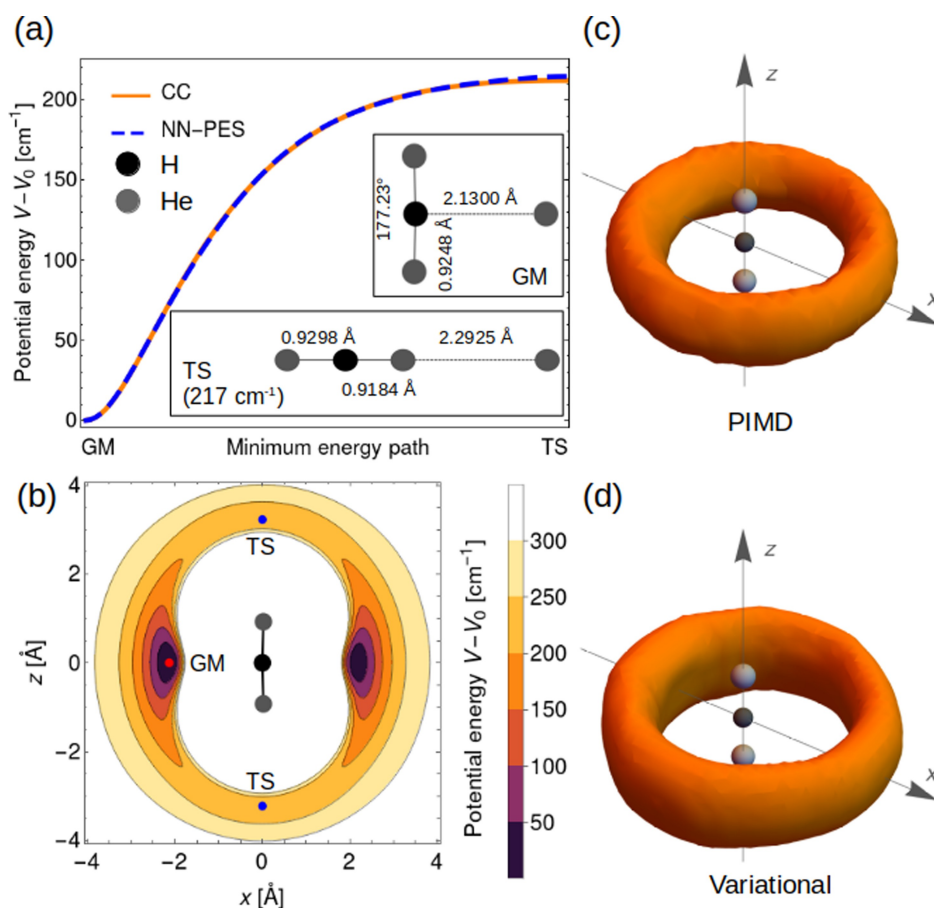


**Figure 1.** (a) Structures corresponding to the stationary points on the potential energy surface (PES) of  $\text{HHe}_3^+$  in the insets (global minimum, GM, and the linear transition state, TS) and the potential energy profile along the minimum-energy path from the GM to the TS given by the neural network (NN) PES and explicit coupled cluster (CC) calculations. For reference, we note that the H–He distance in the linear triatomic molecule  $\text{HHe}_2^+$  is 0.9246 Å. (b) Two-dimensional cut of the NN-PES when the solvating He moves in the  $(xz)$  plane of the slightly bent chromophore  $\text{HHe}_2^+$ . For each  $(x, z)$  position of the solvating He atom, the structure of the chromophore is optimized. (c) Spatial distribution function (SDF) of the solvating He, as obtained from path integral molecular dynamics (PIMD) simulations at a thermodynamic temperature of  $T = 1$  K. (d) Nuclear density (ND) of the solvating He as obtained from the variational vibrational ground-state wave function. In both panels (c) and (d), the solvating He is found to be delocalized around the chromophore forming a torus. Note that the specific reduced-dimensionality representation of the full-dimensional ND in Cartesian space (i.e., the chosen ‘embedding’, see text) has been selected in order to visualize the topology of the most probable structure of  $\text{HHe}_3^+$ , as discussed in the section Results and Discussion (at the same time, we are not visualizing the additional local delocalization of the three atoms of the  $\text{HHe}_2^+$  subunit that is therefore depicted graphically using its most probable collinear configuration within  $\text{HHe}_3^+$ ).

interaction. Similar to SDFs, nuclear densities of the individual atoms can be visualized in a Cartesian coordinate system attached to the molecule (so-called ‘embedding’); for the sake of visualization we use in Figure 1c/d an embedding where the  $xz$  plane is defined by the three strongly bonded atoms of the bent chromophore. Our study finds quantum delocalization of the solvating He atom with respect to the instantaneously bent chromophore in all of the bound and quasi-bound vibrational states. The delocalization of the solvating He for the ground rovibrational state (visualized in Figure 1c and d) shows a torus shape, which means that in the dynamical structure the molecule becomes non-planar as the solvating He orbits the central proton. In this sense the effective ground-state structure is vastly different from the equilibrium one.

In order to investigate nuclear delocalization with predictive accuracy, we have constructed a high-quality, neural-network-based<sup>[21,22]</sup> PES for the ground electronic state that describes, on equal footing, both  $\text{HHe}_3^+$  and  $\text{HHe}_2^+$  (see Sec. SII of the Supporting Information for details and references on this NN-PES-HHE2P-HHE3P-2022-V1 surface, abbreviated as NN-PES in what follows). The NN-PES is based on ‘gold-standard’ electronic-structure theory, benchmarked in Sec. SI1. The most important stationary-point structures on the NN-PES of  $\text{HHe}_3^+$  are the T-shaped global minimum and a collinear first-order transition state (TS), subject to an electronic-energy difference of 217 cm<sup>-1</sup> (see Figure 1a).

The NN-PES allows the elucidation of NQEs on the structural, dynamical, and spectroscopic properties of  $\text{HHe}_3^+$ , and, for reference purposes, of  $\text{HHe}_2^+$ . Converged

PIMD simulations were performed at a temperature of  $T = 1$  K (using the latest techniques as recently reviewed<sup>[23]</sup> and implemented in the CP2k simulation package<sup>[24,25]</sup>), essentially corresponding to the ground state, to investigate SDFs (see Sec. SI2). In addition, converged variational nuclear-motion computations were carried out, using the code GENIUSH,<sup>[26–28]</sup> to compute eigenenergies and eigenfunctions (and thus nuclear densities, NDs) of rovibrational eigenstates not only below but also above the first dissociation limit of  $\text{HHe}_3^+$  (see Sec. SI3–SI7). These highly accurate calculations provide the basis for investigating the delocalization of the solvating He atom of  $\text{HHe}_3^+$ .

## 2. Results and Discussion

To understand the structural properties, the rovibrational energy levels, and then the associated spectra of  $\text{HHe}_3^+$ , one needs, as reference, related information on  $\text{HHe}_2^+$ . The computed rovibrational transitions of  $\text{HHe}_2^+$  exhibit outstanding agreement with their experimental counterparts<sup>[20]</sup> (see Tables SI11 and SI12), verifying the accuracy of the NN-PES. As to the *average* structure of  $\text{HHe}_2^+$  in the vibrational ground state, the expectation values of the bond length and the bond angle are 0.969 Å and 158°, respectively (the equilibrium values are 0.925 Å and 180°, see Figure 1a and its caption); the latter value shows the required<sup>[29]</sup> but unusually pronounced deviation from linearity. At the same time, the *most probable* structure turns out to be linear (according to the underlying quantum probability distribution function depicted in the left panel of Figure SI5). Upon adding the third He atom, the most probable structure of the  $\text{HHe}_2^+$  core within  $\text{HHe}_3^+$  remains linear as shown in the same Figure (and also the average bond angle remains essentially unchanged, see the right panel of Figure SI5).

The most probable structure of a molecule is uniquely defined by the global maximum of the (diagonal of the) many-body nuclear density matrix in its full dimensionality, which is certainly independent from any choice of embedding but difficult to visualize for polyatomics. Thus, one can successively unfold the computed many-body ND by

determining the most probable structure in a series of subspaces.<sup>[10,30]</sup> Starting with the  $\text{HHe}_2^+$  core, the most probable structure is the perfectly collinear arrangement within that subspace of  $\text{HHe}_3^+$ . The most probable location of the third He atom, however, does not turn out to be a point according to our ND analysis, but is given instead by a circular line around the central proton that yields the most probable structure of  $\text{HHe}_3^+$ . This is exactly what we are trying to capture by the specific embedding chosen in Figure 1c/d exclusively in order to visualize the representative ground-state structure of  $\text{HHe}_3^+$ . It is important to realize that this delocalization topology is independent from the specific coordinate system used for visualization in the reduced dimensionality (or embedding) offered by 3D Cartesian space.

Having discussed the structure, let us now analyze the computed eigenenergies of the bound vibrational states of  $\text{HHe}_3^+$ , compiled in Table 1 under ‘Bound states’. Adding a solvating He to linear  $\text{HHe}_2^+$  introduces three degrees of freedom, two vibrational modes and a rotational one, and nonlinearity due to the T-shaped arrangement of the nuclei. The motion of the solvating He atom can be described by three spherical-polar coordinates (marked in blue in Figure SI6). The vdW bend and stretch fundamentals, at 96 and 102  $\text{cm}^{-1}$ , respectively (see Table 1), are associated with the  $\theta$  angle and the  $R$  radial coordinate, respectively. The  $\varphi$  angle, measured from the plane of the instantaneously bent chromophore unit, describes the orbiting motion of the solvating He around the proton of the chromophore. It is important to point out that there are no vdW vibrational states corresponding to this motion: the remaining four bound vibrational states above the two fundamentals can be labeled as vdW bending overtones (see the first column of Table 1). The bound states follow an unusual energy pattern, related to the unusual topology of the PES (see Figure 1b) and the small value,  $D_0 = 170(10) \text{ cm}^{-1}$ , of the first dissociation energy, corresponding to the  $\text{HHe}_3^+ \rightarrow \text{HHe}_2^+ + \text{He}$  reaction. Note also that the bound states, apart from the ground state, which is necessarily totally symmetric, form  $A_1 - B_2$  symmetry pairs (see Table SI9 for the irreducible representations of the appropriate molecular symmetry group,  $S_2^{*(B1)}$ ).

**Table 1:** Energies ( $E$ , in  $\text{cm}^{-1}$ ) of vibrational bound and quasi-bound (resonance) states of  $\text{HHe}_3^+$ , with symmetry labels ( $\Gamma$ ) corresponding to the  $S_2^*$  molecular symmetry group. The vdW energy increments,  $E_{\text{vdW}}$ , are the energy differences between the combination vibration and the corresponding fundamental of the chromophore. For reference, the vibrational fundamentals of  $\text{HHe}_2^+$  are 956.6, 874.9, and 1315.6  $\text{cm}^{-1}$  for the symmetric stretch, bend, and antisymmetric stretch, respectively.

Chrom. vib.	Bound states		In-plane bend			Out-of-plane bend			Symmetric stretch			Antisymmetric stretch		
	$\Gamma$	$E = E_{\text{vdW}}$	$\Gamma$	$E$	$E_{\text{vdW}}$	$\Gamma$	$E$	$E_{\text{vdW}}$	$\Gamma$	$E$	$E_{\text{vdW}}$	$\Gamma$	$E$	$E_{\text{vdW}}$
vdW vib.														
Ground state (experimental)	–			841.8 <sup>a</sup>			887.6 <sup>a</sup>			n.a. <sup>b</sup>			1300.1(1) <sup>c</sup>	
Ground state (computational)	$A_1$	0.0	$A_1$	841.8	0.0	$B_1$	887.6	0.0	$A_1$	949.6	0.0	$B_2$	1295.8	0.0
vdW bend	$B_2$	95.9	$B_2$	960.6	118.8	$A_2$	981.6	94.0	$B_2$	1050.0	100.4	$A_1$	1407.3	111.5
vdW stretch	$A_1$	101.8	$A_1$	958.3	116.5	$B_1$	987.8	100.1	$A_1$	1053.8	104.2	$B_2$	1402.6	106.7
vdW bend overtone	$A_1$	144.0	$A_1$	1022.1	180.3	$B_1$	1034.8	147.1	$A_1$	1100.8	151.2	$B_2$	1459.6	163.8
vdW bend overtone	$B_2$	144.1	$B_2$	1024.2	182.4	$A_2$	1034.9	147.3	$B_2$	1101.3	151.7	$A_1$	1462.1	166.3
vdW bend overtone	$A_1$	170.7	$A_1$	1062.4	220.5	$B_1$	1071.7	184.1	$A_1$	1126.7	177.1	$B_2$	1482.3	186.5
vdW bend overtone	$B_2$	171.3	$B_2$	1062.4	220.6	$A_2$	1071.9	184.3	$B_2$	1127.0	177.4	$A_1$	–	–

<sup>[a]</sup> Ref. [19]. <sup>[b]</sup> Not available experimentally. <sup>[c]</sup> Ref. [20].

Experimental information on the (ro)vibrational states of  $\text{HHe}_3^+$  is limited to fundamentals of its chromophore.<sup>[19,20]</sup> The four vibrational fundamentals, namely the in-plane (IPB) and out-of-plane (OPB) bends and the symmetric and antisymmetric stretches, lie well above  $D_0$ ; therefore, they correspond to quasi-bound (resonance) states.<sup>[32]</sup> These fundamentals show the perturbed features of a solvated linear triatomic molecule with a significantly split bending. Since the coupling of the ‘intramolecular’ motions with the ‘intermolecular’ dissociation is very inefficient (their time and energy scales are very different), the lifetimes of many resonance states of  $\text{HHe}_3^+$  are relatively long, allowing their detection in spectroscopic measurements<sup>[19,20]</sup> (see also the first row of Table 1). The wave functions of these resonances resemble those of bound states (see Figure SI10). The computed fundamentals, see the second row of Table 1, closely match the three available experimental ones, confirming the outstanding accuracy of the NN-PES also for  $\text{HHe}_3^+$ .

Among the large number of quasi-bound vibrational states computed, we could identify states which include excitation both in the chromophore and the vdW modes. The energies of these combination modes are also given in Table 1. The same vdW vibrations can be identified in these combination modes as for the bound states. In order to facilitate the assessment of the coupling between the vdW and chromophore vibrations, we also report  $E_{\text{vdw}}$  energy increments. These are differences between the eigenenergies of the combination modes and the corresponding vibrational fundamental of the chromophore (see Table 1), which can straightforwardly be compared with the bound-state energies.

After investigating the bound as well as the long-lived resonance states of  $\text{HHe}_3^+$ , let us return to the effective structure of this vdW complex. The most notable feature of  $\text{HHe}_3^+$  in the ground vibrational state, confirmed both by SDF and ND analyses as presented in Figures 1c and d, respectively, is the delocalization of the solvating He atom. It is important to emphasize that the quantum nuclear delocalization of the solvating He atom has nothing to do with the rotation of the entire  $\text{HHe}_3^+$  molecule (the NDs depicted in Figures 1 and 2 strictly correspond to  $J = 0$  wave functions, where  $J$  is the quantum number corresponding to the overall rotation of  $\text{HHe}_3^+$ ). Rather, as the molecule vibrates, many configurations of  $\text{HHe}_3^+$  are populated in which the  $\text{HHe}_2^+$  unit is bent (note that the expectation values of the chromophore’s bond length and bond angle in  $\text{HHe}_3^+$  are very similar to those of bare  $\text{HHe}_2^+$ ); therefore, we can define an angle ( $\phi$ ) between the plane of the instantaneously bent chromophore and the solvating He. For the ground state, the probability density along  $\phi$  is almost constant (*vide infra*), which manifests in the torus-type delocalization of the solvating He.

The above discussion is useful for states other than the vibrational ground state. All the bound vibrational states, corresponding to excitation of the vdW modes, exhibit not only torus-type delocalization of the solvating He but also nodal surfaces in their state-specific NDs (see Figure 2a and b for the vdW bend and stretch fundamentals, respectively):

we find nodal surfaces along  $\theta$  and  $R$  for the bound vdW bend and stretch fundamentals, respectively (see Figure SI10 for the analyses of additional states). The next important observation is that the NDs of the solvating He corresponding to the quasibound bending fundamental modes of the chromophore also contain nodes, but this time along  $\phi$  (see Figure 2c and d). In the case of the OPB bend, it is the nodal plane defined by the chromophore, while the ND of the IPB has a perpendicular nodal plane. Clearly, the bending motions of the chromophore involve excitation of the solvating He along the  $\phi$  coordinate. For the symmetric and antisymmetric stretch fundamentals of the chromophore the ND of the solvating He atom is a torus, similar to that of the ground state, since the excitation does not involve the solvating He (see Figure SI10).

An effective Hamiltonian (EH) model,<sup>[33]</sup> discussed in detail in Sec. SI8, is able to explain qualitatively the structure of the NDs of the solvating He atom for the bound and quasibound states. This EH model restricts motion to the bending of the  $\text{HHe}_2^+$  chromophore and the vdW bending of  $\text{HHe}_3^+$ . The vdW bending is treated as an internal rotation of the instantaneous bent chromophore, hindered by an anisotropic intermolecular potential. Excitation of the degenerate bending of the linear chromophore induces angular momentum. If  $\nu$  is the total number of excitations in the bending mode, then  $k = -\nu, -\nu + 2, \dots, \nu - 2, \nu$  is the angular momentum quantum number. If the intermolecular  $\text{HHe}_2^+ \dots \text{He}$  potential does not depend on  $\phi$  and the  $l$ -type doubling is neglected (see the SI), then the wave function of  $\text{HHe}_3^+$  along  $\phi$  can be approximated as  $\Psi(\phi) \approx \exp(ik\phi)$ , similar to the particle-on-a-ring model (note that the coordinates of the EH model differ slightly from the spherical polar coordinates of the solvating He atom introduced earlier; this is why the formula for  $\Psi(\phi)$  is only an approximation). If bending of the chromophore is not excited, then  $\nu = 0$  and thus  $k = 0$ . Therefore, the absolute value of the wave function along coordinate  $\phi$  is approximately constant and we observe a torus in the ND of the solvating He atom. This EH model also facilitates our understanding of the nature of the bending fundamentals of the chromophore. In the case of IPB and OPB,  $\nu = 1$ , and thus  $k = \pm 1$ , and the  $\phi$ -dependent part of the potential and the  $l$ -type doubling term couple  $k = +1$  with  $k = -1$ . Thus, the wave function will have  $\Psi(\phi) \approx \cos(\phi)$  and  $\Psi(\phi) \approx \sin(\phi)$  form for IPB and OPB, respectively, which then fully explains the observed nodal structures of the in- and out-of-plane bend fundamentals (see Figure 2).

Next, let us investigate further the effect of delocalization on the energies of the bound states and the  $E_{\text{vdw}}$  energy increments (see Sec. SI6 for details). If the chromophore is bent, the cylindrical symmetry of the potential is lost and the energies of the bound states and the  $E_{\text{vdw}}$  energy increments will depend on the angle  $\phi$ . Figure 2e indeed shows significant changes in the  $E(\phi)$  energies of the bound states obtained from reduced-dimensional computations, whereby  $\phi$  is fixed at different values (the  $E_{\text{vdw}}(\phi)$  energy increments corresponding to the chromophore’s quasibound combination vibrations behave similarly, see Figure SI7). Despite the pronounced  $\phi$  dependence, the arithmetic averages of the

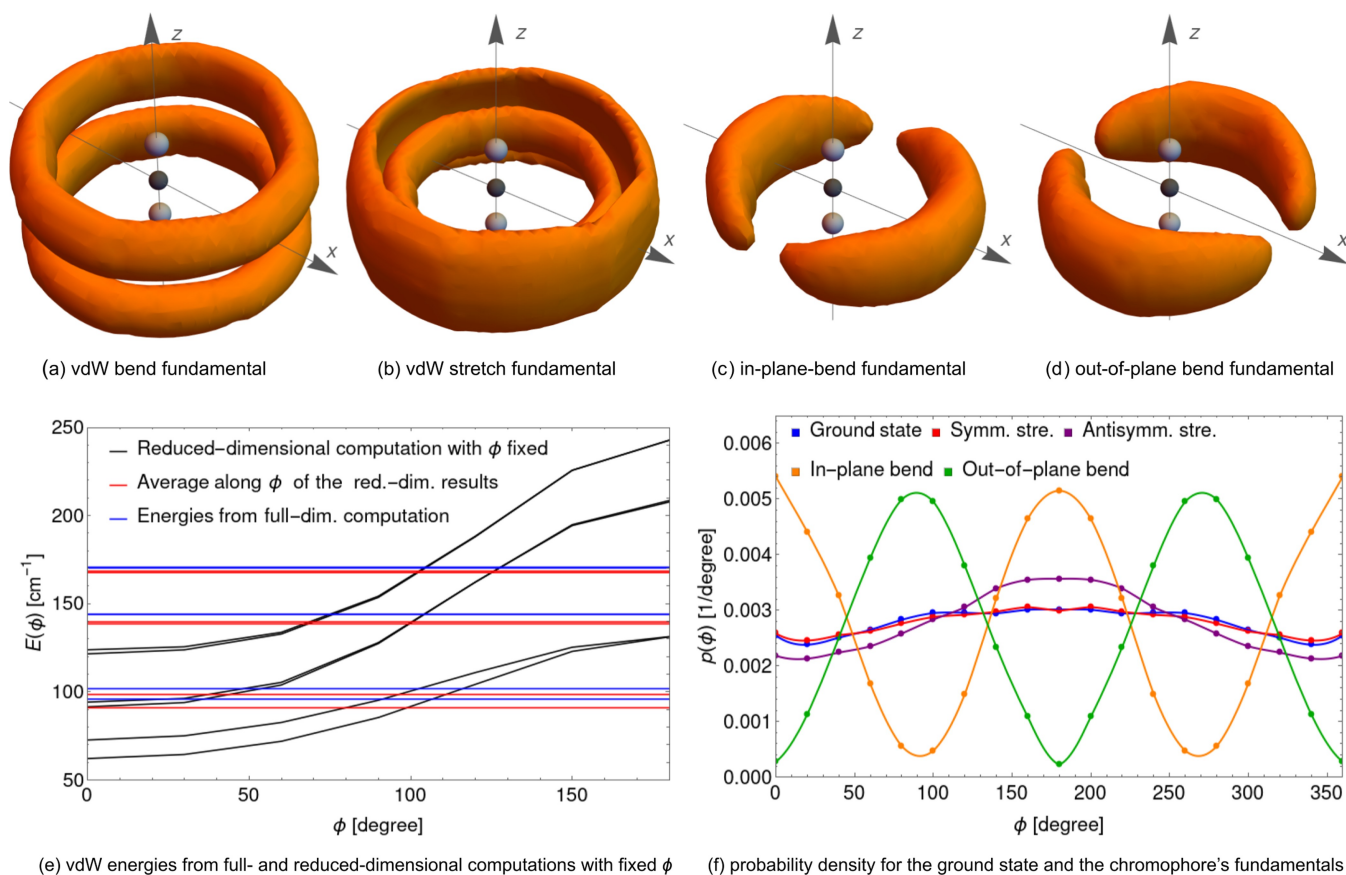


**Figure 2.** (a)–(d) Nuclear densities of  $\text{HHe}_3^+$  obtained from the variational wave functions of excited vibrational states below and above the first dissociation limit in panels (a)–(b) and (c)–(d), respectively (see Figure 1d for the ground state). The body-fixed  $xyz$  coordinate system is defined such that the flexible  $\text{HHe}_2^+$  core is in the  $xz$  plane with the proton at the origin, the bisector of the bond angle is on the  $x$  axis, and the core is only allowed to bend in the  $+x$  direction. Panels (a)–(d) show that the solvating He is delocalized around the  $\text{HHe}_2^+$  moiety in a torus-like manner (much like in the node-free ground state). The four distinct nodal structures of the nuclear densities reflect specific types of vibrational excitation of  $\text{HHe}_2^+$ . (e) Role of the torus-like delocalization of the solvating He on the bound-state (vdW) energies.  $E(\phi)$ : vdW energies obtained from reduced-dimensional computations with  $\phi$  fixed to different values (black curves) along half of its interval and  $\phi$  fixed to its expectation value,  $158^\circ$ . The arithmetic averages of the  $E(\phi)$  energies over  $\phi$  (red horizontal lines) agree well with the 6D (full-dimensional) bound-state energies (blue horizontal lines). (f) Probability densities of  $\phi$ ,  $p(\phi)$ , for the ground state and the four “intramonomer” fundamentals; in particular,  $p(\phi) \approx \cos^2(\phi)$  for the in-plane bend fundamental and  $p(\phi) \approx \sin^2(\phi)$  for the out-of-plane bend fundamental, while  $p(\phi)$  is approximately constant for vibrational states not involving intramonomer bending excitation.

$E(\phi)$  energies for the bound states reproduce the full-dimensional results for the vdW bound states (Figure 2e), showing the averaging effect of the torus.

Probability densities of  $\phi$ ,  $p(\phi)$ , for the ground state and the four fundamentals corresponding to the chromophore have also been computed from the full-dimensional eigenfunctions, the results are shown in Figure 2f. Note that  $p(\phi)$  is almost constant for all the bound states, in line with the toroidal structure of the NDs. The different  $E_{\text{vdW}}$  increments corresponding to the four chromophore modes, given in Table 1, can be also explained by combining the different probability densities with the energy curves given in Figure 2e. For example,  $p(\phi)$  for the antisymmetric stretch is larger at  $\phi = 180^\circ$  and smaller at  $\phi = 0^\circ$  than for the ground state. Therefore, the full-dimensional  $E_{\text{vdW}}$  energy increments for the antisymmetric stretch will be larger than their counterparts for the bound states (cf. columns ‘Bound states’ and ‘Antisymmetric stretch’ of Table 1). The distinctly

different  $E_{\text{vdW}}$  increments for the in- and out-of-plane bendings are also explained by the vastly different probability densities  $p(\phi)$ . Note also the mutual support of the EH model and the  $p(\phi)$  for the IPB and OPB NDs.

### 3. Conclusions

Based on a high-quality neural network potential energy surface constructed as part of this project, we investigated the nuclear dynamics of the  $\text{HHe}_3^+$  van der Waals complex via PIMD simulations and variational nuclear-motion computations. The computed vibrational energy levels have outstanding agreement with the available experimental spectroscopic data. We investigated the dynamical structure by calculating the spatial distribution functions (SDF) at  $T = 1$  K and nuclear densities (ND) corresponding to vibrational states below and above the dissociation limit. We

focused on the delocalization of the solvating He atom with respect to the strongly-bound quasi-linear  $\text{HHe}_2^+$  core (“chromophore”). We found that as the molecule vibrates, the solvating He atom is not restricted to stay in the plane of the instantaneously bent chromophore, instead, it orbits around the central proton almost freely, producing a torus-type delocalization seen both on the SDF and ND plots (this is seen for all the van der Waals and intramolecular vibrational states studied). Note that this phenomenon resembles what was observed for protonated acetylene.<sup>[10]</sup> Another interesting result of this study is that the in-plane and out-of-plane bending vibrations of the chromophore involve excitation along the torus coordinate. It is also important to emphasize that simple models can be devised which explain the different delocalization patterns of the solvating He. The phenomena observed in this work are expected to appear for other systems, as well, where a linear (triatomic) molecule is solvated by an atom in a nonlinear fashion.

### Acknowledgements

IS and AGC are grateful to NKFIH for support (grants ÚNKP-20-3, ÚNKP-21-3, and K138233). The Bochum research has been partially funded by the Deutsche Forschungsgemeinschaft (DFG, German Research Foundation) under Germany's Excellence Strategy – EXC 2033–390677874 – RESOLV and via grant MA 1547/19-1 with computational resources provided by HPC–RESOLV, HPC@ZEMOS, and BoViLab@RUB. CS acknowledges partial financial support from the Alexander von Humboldt Stiftung and the DFG - 500244608. The Köln team has been supported by DFG via SFB 956 (project ID 184018867) and grants AS 319/2-2 and SCHL 341/6-2. This publication supports research performed within the COST Action CA21101 “Confined molecular systems: from a new generation of materials to the stars” (COSY), funded by the European Cooperation in Science and Technology (COST). The authors are grateful to the referees for their insightful comments.

### Conflict of Interest

The authors declare no known conflict of interest.

### Data Availability Statement

The data that support the findings of this study are available in the supplementary material of this article.

**Keywords:** nuclear delocalization · variational nuclear-motion computations · path integral molecular dynamics (PIMD) · spatial distribution functions (SDF) · nuclear density (ND)

- [1] A. Streitwieser, C. H. Heathcock, E. M. Kosower, *Introduction to Organic Chemistry*, 4th ed., Pearson College Div, **1980**.
- [2] R. P. Bell, *The Tunnel Effect in Chemistry*, Springer, Berlin, **1980**.
- [3] P. R. Schreiner, H. P. Reisenauer, *Angew. Chem. Int. Ed.* **2008**, *47*, 7071–7074.
- [4] P. R. Schreiner, H. P. Reisenauer, F. C. Pickard, A. C. Simmonett, W. D. Allen, E. Mátyus, A. G. Császár, *Nature* **2008**, *453*, 906–909.
- [5] C. Castro, W. L. Karney, *Angew. Chem. Int. Ed.* **2020**, *132*, 8431–8442.
- [6] T. Schleif, M. Prado Merini, W. Sander, *Angew. Chem. Int. Ed.* **2020**, *59*, 20318–20322.
- [7] T. E. Markland, M. Ceriotti, *Nat. Rev. Chem.* **2018**, *2*, 0109.
- [8] M. W. Crofton, M. Jagod, B. D. Rehfuß, T. Oka, *J. Chem. Phys.* **1989**, *91*, 5139–5153.
- [9] D. Marx, M. Parrinello, *Science* **1996**, *271*, 179–181.
- [10] L. Knoll, Z. Vager, D. Marx, *Phys. Rev. A* **2003**, *67*, 022506.
- [11] E. T. White, J. Tang, T. Oka, *Science* **1999**, *284*, 135–137.
- [12] O. Asvany, P. Kumar, B. Redlich, I. Hegemann, S. Schlemmer, D. Marx, *Science* **2005**, *309*, 1219–1222.
- [13] S. D. Ivanov, O. Asvany, A. Witt, E. Hugo, G. Mathias, B. Redlich, D. Marx, S. Schlemmer, *Nat. Chem.* **2010**, *2*, 298–302.
- [14] I. Simkó, C. Fábri, A. G. Császár, *J. Chem. Theory Comput.* **2023**, *19*, 42–50.
- [15] D. Marx, M. E. Tuckerman, J. Hutter, M. Parrinello, *Nature* **1999**, *397*, 601–604.
- [16] D. Marx, M. Parrinello, *J. Chem. Phys.* **1996**, *104*, 4077–4082.
- [17] D. Marx, J. Hutter, *Ab Initio Molecular Dynamics: Basic Theory and Advanced Methods*, Cambridge University Press, **2009**.
- [18] A. G. Császár, T. Szidarovszky, O. Asvany, S. Schlemmer, *Mol. Phys.* **2019**, *117*, 1559–1583.
- [19] O. Asvany, S. Schlemmer, T. Szidarovszky, A. G. Császár, *J. Phys. Chem. Lett.* **2019**, *10*, 5325–5330.
- [20] M. Töpfer, A. Jensen, K. Nagamori, H. Kohguchi, T. Szidarovszky, A. G. Császár, S. Schlemmer, O. Asvany, *Phys. Chem. Chem. Phys.* **2020**, *22*, 22885–22888.
- [21] J. Behler, *Angew. Chem. Int. Ed.* **2017**, *56*, 12828–12840.
- [22] J. Behler, *Chem. Rev.* **2021**, *121*, 10037–10072.
- [23] F. Brieuç, C. Schran, F. Uhl, H. Forbert, D. Marx, *J. Chem. Phys.* **2020**, *152*, 210901.
- [24] J. Hutter, M. Iannuzzi, F. Schiffmann, J. Vandevondele, *WIREs Comput. Mol. Sci.* **2014**, *4*, 15–25.
- [25] CP2k Open Source Molecular Dynamics, www.cp2k.org.
- [26] E. Mátyus, G. Czakó, A. G. Császár, *J. Chem. Phys.* **2009**, *130*, 134112.
- [27] C. Fábri, E. Mátyus, A. G. Császár, *J. Chem. Phys.* **2011**, *134*, 074105.
- [28] C. Fábri, M. Quack, A. G. Császár, *J. Chem. Phys.* **2017**, *147*, 134101.
- [29] T. Hirano, U. Nagashima, P. Jensen, *J. Mol. Spectrosc.* **2018**, *343*, 54–61.
- [30] R. Beckmann, R. Topolnicki, D. Marx, *J. Phys. Chem. A* **2023**, *127*, 2460–2471.
- [31] P. R. Bunker, P. Jensen, *Molecular Symmetry and Spectroscopy*, NRC Research Press, Ottawa, **2006**.
- [32] A. G. Császár, I. Simkó, T. Szidarovszky, G. C. Groenenboom, T. Karman, A. van der Avoird, *Phys. Chem. Chem. Phys.* **2020**, *22*, 15081–15104.
- [33] Y. Ohshima, Y. Matsumoto, M. Takami, K. Kuchitsu, *J. Chem. Phys.* **1993**, *99*, 8385–8397.

Manuscript received: May 15, 2023

Accepted manuscript online: August 10, 2023

Version of record online: August 31, 2023